Chapter 3

3.1 Introduction

The synthesis and characterizations of materials are the primary and important step in the experimental research. The behavior of samples mainly depends on its method of preparation. There are many experimental procedures for preparation of multiferroics at macroscopic level such as solid-state reaction method, Sol-gel auto combustion route, Liquid phase sintering, Spark plasma sintering etc. The routes such as rapid phase/microwave sintering and sol-gel combustion route processing methods are not cost effective by view of industrial scale production. The conventional solid-state reaction method is relatively cost effective and easy. It also leads to uniform mixing of the metal oxides and carbonates. However, some drawbacks of this method are there such as major impurity phases, poor sintering behavior due to non-uniformity of particle size and shape, multiphase character, lack of reproducibility, and loss of stoichiometry.

Our focus laid on the research related with structural, electrical and magnetic properties of bulk BFO prepared by mechno-chemical solid-state route. In this method high energy ball mill is used for atomic scale mixing of the ingredients, thus forming a homogenous amorphous mixture and calcination temperature could be significantly lowered.

3.1.1 Raw materials: The chemicals used in this work are as follows: Bi_2O_3 (99.7%), Sm_2O_3 (99.9%), Fe_2O_3 (97%), Gd_2O_3 (99.6%), MgO (99.8%), TiO_2 (99.5%), $BaCO_3$ (99.7%), ZrO_2 (99.8%). All the chemicals were purchased from Loba Chemie Pvt. Ltd.

3.1.2 Experimental procedure

Bismuth ferrite based polycrystalline samples were prepared by solid state route. The stoichiometric amount of raw materials were taken; mixed and grounded for 16 hours using high energy ball mill (Insmart technology planetary high energy ball mill). After powders were dried at 120 °C in hot air oven and then calcined at 750°C for 2 hours. The calcined powders were grounded in the ball mill. The fine powders were mixed with PVA binder and pressed into cylindrical pellets of 10 mm in diameter and 1.5mm - 2mm in thickness using a hydraulic press with a pressure of 6 KN. During sintering, the temperature for samples were varied at the rate of 5 °C/min up to 400 °C and hold for 2 hours for binder removal and then rate was increased to 2 °C/min up to sintering temperature (830 °C) and hold for 1 hour. The calcination and sintering routes are shown in fig.3.1 (a and b). The flowchart of the complete experimental process is shown in fig.3.2.

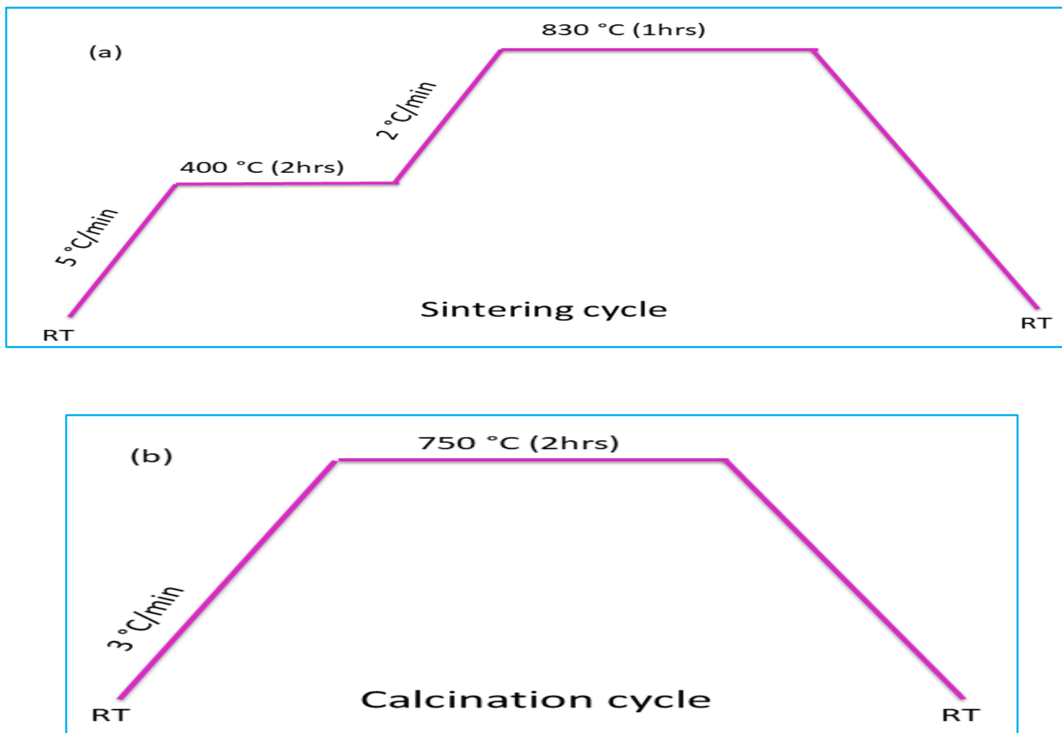

Fig. 3.1: Sintering and Calcination routes.

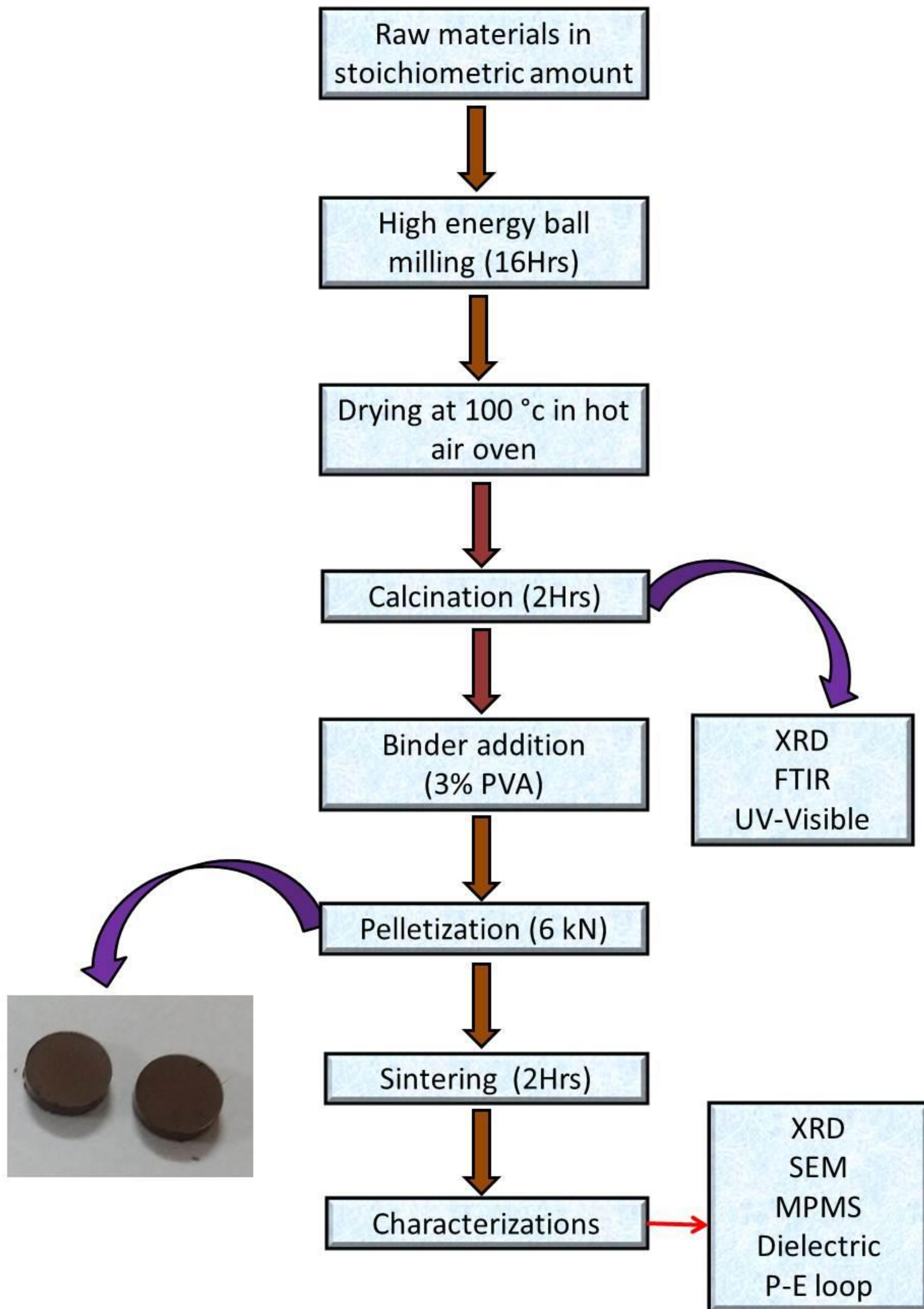

Fig. 3.2: Flowchart of experimental procedure.

3.2 Characterizations

3.2.1 Density measurement

After sintering of samples density measurement is the first step. Bulk density of the samples is measured by density measurement kit (Sartorius, BSA2245CW). The principle of density measurement is based on Archimede's principle. The sample weight has been measured using a weighing balance having accuracy of 0.0001 g. The submerged liquid for density measurement was water of density $1 g/cm^3$.

The bulk density (B_d) is measured by the following formula:

$$B_d = \frac{W_d \times \rho_w}{W_S - W_h} \tag{3.1}$$

Where, W_d is dry weight, ρ_w is the density of water. W_S is soaked weight that means weight of the samples after keeping them in water for two hours under vacuum atmosphere and W_h is suspended weight of the prepared sample.

3.2.2 Structural analysis

3.2.2.1 X-ray Diffraction

The X-rays are electromagnetic radiations and having wavelength in the range of 0.01-10 nm. X-rays are produced when an electromagnetic radiation of sufficient energy bombarded with an atom which knock out an electron from the K-shell and the vacancy of electron is filled with any electron of outer orbitals (L, M) and the photon of energy emit an X-ray. The mechanism of production of X-ray is shown in Fig. 3.3. These radiations have dual (wave/particle) nature. The X-rays have smaller wavelength and higher energy as compared to visible light and also have ability of penetration into the matter however; it is

dependent of density of the material. Therefore, the X-ray diffraction is used for investigation of structure of an atom. The detection limit of XRD is ~1-4%.

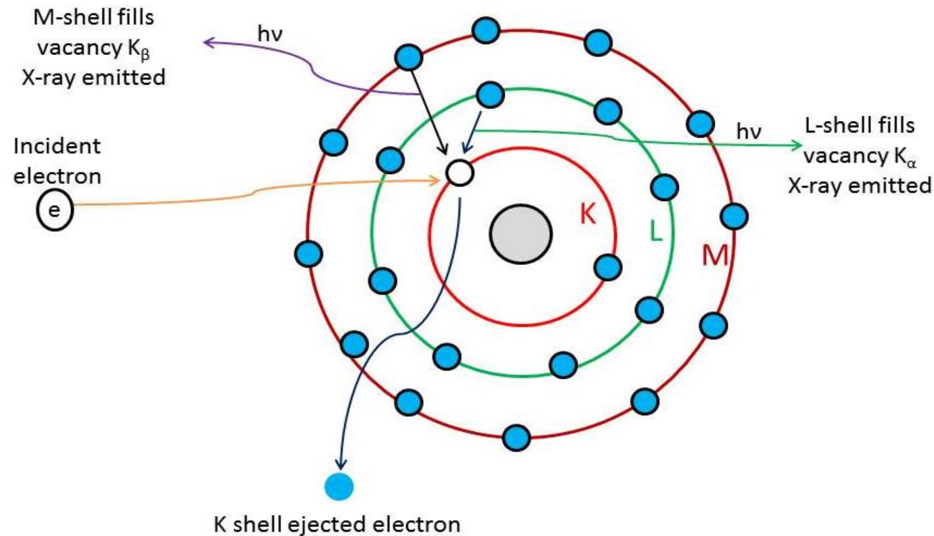

Fig. 3.3: X-Rays production from an atom.

X-ray diffraction is a nondestructive technique generally used for the detailed structural analysis of crystalline compounds. The diffraction pattern is obtained when an incident monochromatic X-ray beam is interacts with the atoms of the target material and produces constructive interference by satisfying the Braggs law:

$$n\lambda=2d\sin\theta \qquad (3.2)$$

where, n is an integer, λ is the characteristic wavelength of the X-rays impinging on the crystallize sample, d is the interplanar spacing between rows of atoms, and θ is the angle of the X-ray beam with respect to these planes.

$$\frac{1}{d_{hkl}^2}=\frac{4}{3}\left(\frac{h^2+k^2+hk}{a^2}\right)+\left(\frac{l^2}{c^2}\right) \qquad (3.3)$$

The principle of X-ray diffraction is shown by Fig. 3.4.

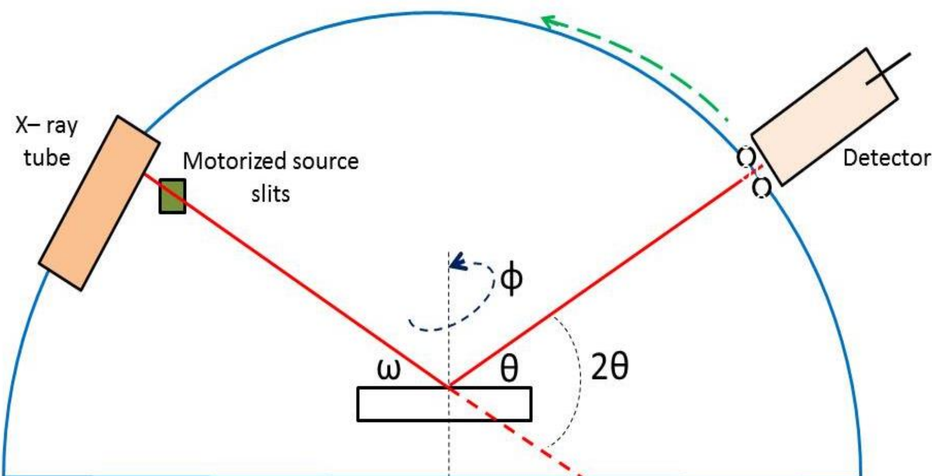

Fig. 3.4: Principle of X-ray diffraction (Prof. Thomas Key)

For copper as target material, K_{α} having wavelength (λ) = 1.54059Å. The operating voltage for diffractometer is 30 kV and current are 30 mA.

In the present work the instrument used for X-ray diffraction data recording is bench top (RIGAKU-Miniflex II HD20972, Japan). The sintered pellets were placed in quartz sample holder. The software used to run the diffractometer was Smart Lab. The diffracted intensity measured in steps of 0.02° at a speed of 5° per minute across the range of 2θ =10° - 80°. The subsequent data was analyzed using the computer program "PDXL2".

3.2.2.2 Rietveld Refinement

The sintered powdered samples were measured in HR-XRD instrument (RIGAKU-Smart Lab 9kW Powder type). The samples were exposed with copper target and recorded at range of 2θ = 10° – 90° with a scanning rate 2°/min at a step of 0.01. The recorded data were analyzed with Rietveld refinement "FullProf" software. Rietveld method uses the non-linear

least square method and the measured data is compared with standard crystallographic database.

The structure of a powder diffraction pattern is obtained with instrumental parameters and two crystallographic parameters. Instrumental parameters are as follows for Peak position: wavelength, axial divergence of the beam and sample alignment; for Peak intensity: Geometry and configuration, radiation (Lorentz Polarization); for Peak shape: Radiation, geometry, Beam conditioning. Crystallographic parameters are unit cell dimensions, and atomic content and coordination. So, the powder model is established as:

Peak shape functions (PSF): Irrespective of the software, for general applications of Rietveld refinement, the Bragg peaks are well defined with peak shape functions which includes convolution (©) of three functions; instrumental broadening Ω(θ), wavelength dispersion Λ(θ), and the specimen function Ψ(θ), with the addition of a background function, b(θ).

$$PSF(\theta) = \Omega(\theta) © \Lambda(\theta) © \Psi(\theta) + b(\theta) \quad (3.4)$$

Other parameters like average crystallite size, D, and microstrain, ξ, effects on Bragg peak broadening, β (in radians), can be described as follows, where k is a constant:

$$\beta = \frac{k\lambda}{D.cos\theta} \quad (3.5)$$

The pseudo-Voigt profile is the most common and is the basis for most PSF's. The pseudo-Voigt function can be represented as:

$$y(x) = V_p(x) = n * G(x) + (1 - n) * L(x) \quad (3.6)$$

Where: *G(x)* and *L(x)* Gaussian and Lorentzian contributions, respectively. Normalization of Gaussian and Lorentzian function is given by:

$$\int_{-\infty}^{\infty} G(x)d(x) = 1\ ,\ \int_{-\infty}^{\infty} L(x)d(x) = 1 \qquad (3.7)$$

In pseudo-Voigt profile for Gauss function, FWHM varies with θ and calculated by Caglioti formula [Caglioti *et al*. 1958]:

$$(\beta)^2 = Utan^2\theta + Vtan\theta + W \qquad (3.8)$$

Where: *U*, *V*, *W*, are shape parameters.

For Lorentzian function, FWHM varies with 2θ as derived in equation

$$(\beta)' = \frac{X}{cos\theta} + Ytan\theta \qquad (3.9)$$

Where: X and Y are free variables.

Principle of Rietveld: In this method a residual function (R_f) is minimized to analyze the difference between observed data and calculated data as shown in equation

$$R_f = \sum_i w_i \left\{ y_i^{Obs} - \frac{1}{s_f} y_i^{Cal} \right\} \qquad (3.9)$$

Where, W_i is the statistical weight and s_f is an overall scale factor $y^{cal} = y^{obs}$

Since Rietveld refinement is depends on the best fitting of experimental and calculated patterns which can be quantitatively calculated on the basis Fig.s of merit which have numerical values that specifies the quality of fitting.

Profile residual factor (R_p):

$$R_p = \sum_i^n \frac{\left|Y_i^{obs} - Y_i^{cal}\right|}{\sum_i^n Y_i^{obs}} \times 100\% \qquad (3.10)$$

Weighted profile residual (R_{wp}):

$$R_{wp} = \sum_i^n \left(\frac{w_i\left(Y_i^{obs} - Y_i^{cal}\right)^2}{\sum_i^n w_i\left(Y_i^{obs}\right)^2} \right)^{\frac{1}{2}} \times 100\% \qquad (3.11)$$

Bragg residual (R_B):

$$R_B = \sum_j^m \frac{\left|I_j^{obs} - I_j^{cal}\right|}{\sum_i^n I_j^{obs}} \times 100\% \qquad (3.12)$$

Expected profile residual (R_{exp}):

$$R_{exp} = \left(\frac{n-p}{\sum_i^n w_i\left(Y_i^{obs}\right)^2} \right)^{\frac{1}{2}} \times 100\% \qquad (3.13)$$

Goodness of Fit (χ^2):

$$\chi^2 = \sum_i^n \frac{\left(Y_i^{obs} - Y_i^{cal}\right)^2}{n-p} = \left(\frac{R_{wp}}{R_{exp}}\right)^2 \qquad (3.14)$$

For best fitting goodness of fit should be approached to unity and also visual analysis of difference between observed and calculated data plot.

3.2.3 Optical Studies

3.2.3.1 Fourier–transform Infrared Spectroscopy

Fourier–transform Infrared Spectroscopy (FTIR) is a technique in which a compound (solid, liquid, and gas) exposed with an Infrared radiation (IR) of sufficient energy, the molecules of

the compound resulting in vibration due to excitation from ground state to higher energy state when they absorb IR as shown in Fig. 3.5. These vibrations giving rise to closely absorption bands known as IR absorption spectrum. The band corresponds to the characteristic functional groups and the bond present in the compounds. Michelson interferometer is used as a detector in FTIR. The range of detection limit for FTIR technique is 2.5 to 25μm.

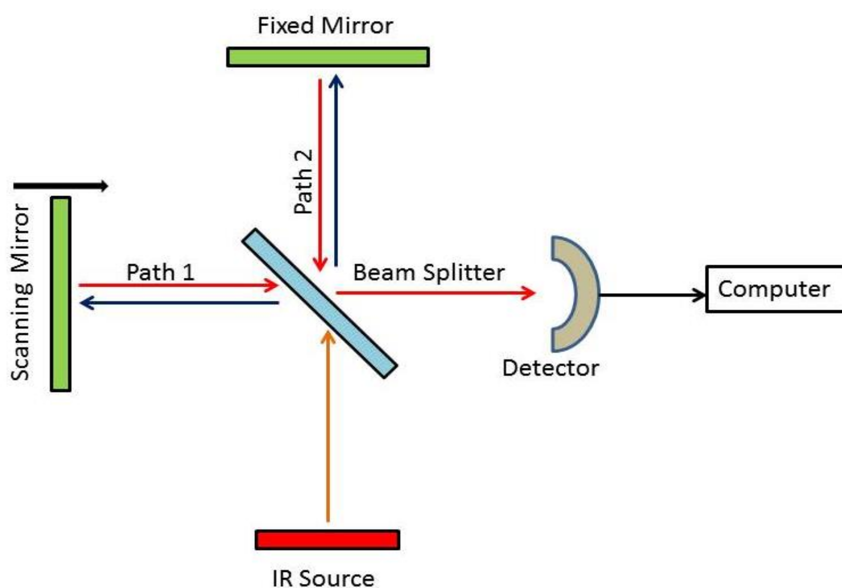

Fig. 3.5: Working principle of FTIR.

In the present study we performed the measurement by placing the calcined powder on the quartz base and data recorded in transmittance mode in the range of wavelength $2.5 \times 10^{-3} - 2.5 \times 10^{-4}$ cm by using Perkin Elmer BXIII, FTIR spectrophotometer with resolution 4 cm^{-1}.

3.2.3.2 Ultraviolet visible Spectroscopy

It is a technique in which light of ultra–violet region (200–400 nm) is absorbed by the molecules. The principle of UV–spectroscopy is based on Beer–Lambert law which states

that "when a beam of monochromatic light is passed through a solution of an absorbing substance, the rate of decrease of intensity of radiation with thickness of the absorbing solution is proportional to the incident radiation as well as the concentration of the solution" as shown in fig. 3.6. The expression of Beer–Lambert law is:

$$Absorbance = \log(I_i/I_c) = m_a m_c L \quad (3.15)$$

Where, I_0 = intensity of light incident upon sample cell, I = intensity of light leaving sample cell, m_c = molar concentration of solute, L = length of sample cell (cm), m_a = molar absorptivity.

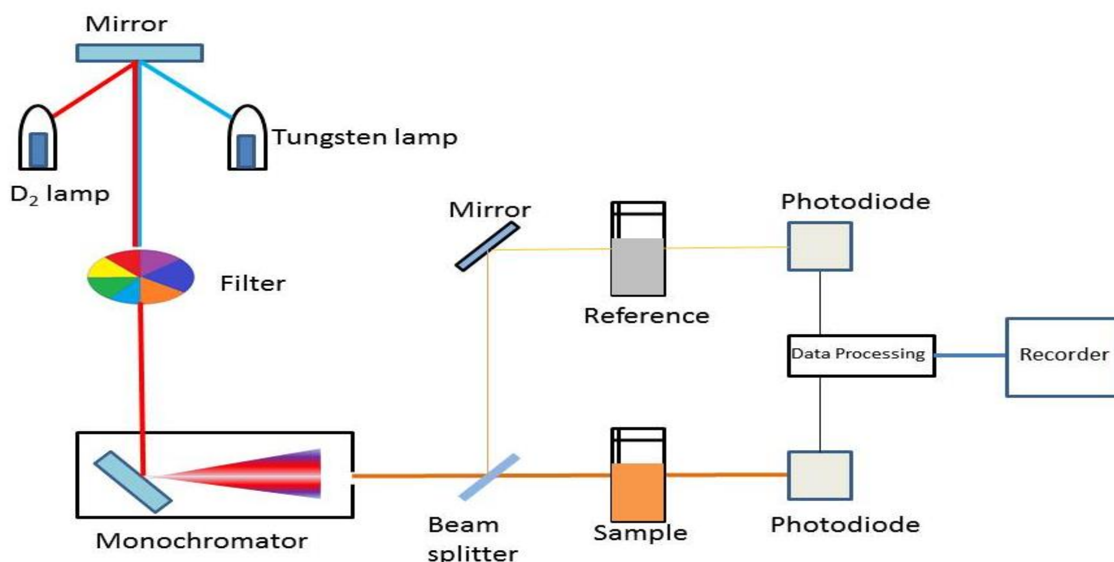

Fig. 3.6: Principle of UV-Visible spectroscopy.

In this thesis we have obtained the UV spectra of calcined powder filled in a quartz cuvette and data is recorded in the wavelength range 200 Å - 1400 Å using SHIMADZU, UV–2600, Japan, UV visible spectrophotometer.

3.2.4 Microstructural studies

3.2.4.1 Scanning Electron Microscopy

Scanning electron microscopy is a technique in which electron from a source interacts with the atoms of the compound and the emitted electrons from the samples produce the information of composition and surface topography. In this work FESEM is used for imaging and elemental analysis because FESEM has higher resolution than conventional SEM.

The mechanism of FESEM is shown in Fig. 3.7. It is based on the principle that an electron gun which is associated with a cathode emission tube produces a narrow beam of electron (usually 5-100 KeV), usually electron source is a heated tungsten or field emission filament. The stream of electron accelerated in vacuum towards the specimen using a positive electrical potential. On the basis of bombardment different type of electrons (secondary electrons (SE), reflected or back-scattered electrons (BSE), characteristic X-rays and light (cathodoluminescence) (CL), absorbed current (specimen current) and transmitted electrons) are emitted from the source.

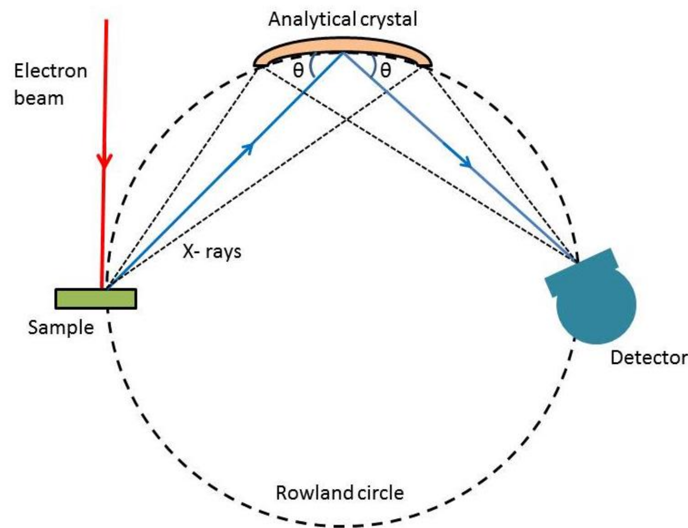

Fig. 3.7: Principle of SEM.

This beam confined to a monochromatic beam as per the requirement of user and focused using metal apertures, on the samples using electromagnetic lenses. The electron beam's interaction and effects occur inside the samples are detected.

In the present study the FESEM was Nova Nano SEM 450 (FEI USA (S.E.A.) The source of electrons was tungsten filament. The sintered pellets of 10 mm diameter were gold sputter coated for 2 minutes at 50Hz frequency and 20 mA current with Desk sputter coater DSR 1. The electron beams were detected using an Everhart-Thornley detector. The detection limit of the instrument is100 nm.

The micrographs produced with the FESEM were analyzed using an image visualization software Image-J developed by Upper Austria University of Applied Sciences.

3.2.4.2 Energy Dispersive Spectroscopy EDS

It is a technique for quantitative analysis of elements of a sample. The fig. shows the EDS image of pure BFO sample. In this work we used "Team Pegasus Integrated EDS-EBSD with Octane Plus and Hikari Pro (*EDAX* Inc." system for elemental analysis as shown in fig. 3.7.

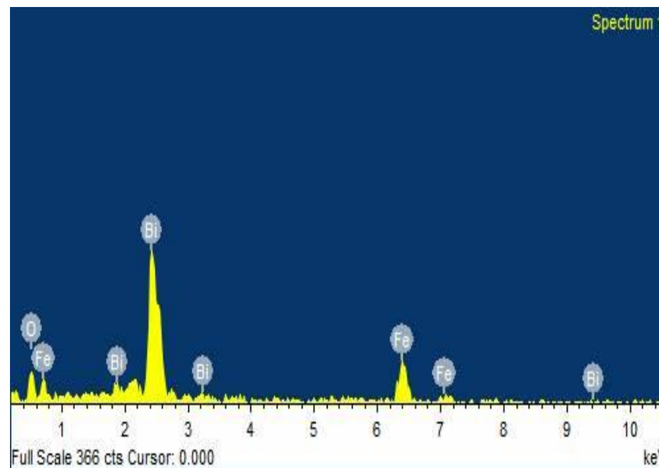

Fig. 3.8: EDS image of BFO.

3.2.4.3 Elemental mapping by EDS

Elemental mapping is an image that shows 2-dimensional spatial distribution of elements that present in compound. Resolution depends on beam size, how long time the beam dwells on each point and concentration of elements.

3.2.3 Dielectric analysis

Dielectric analysis refers to group of measurement techniques in which different properties of a polar material, such as polarization, dielectric permittivity, ac conductivity, dielectric loss, and impedance can be determined as a function of temperature or frequency.

When an electric field is applied to any material displacement current and polarization current are induced in it. For a dielectric material, polarization current is larger than the displacement current. In the polarization current, a positive (+q) and negative (-q) charge shifts to a fixed distance ($\vec{d}$) which is known as dipole; and the moment ($\vec{p}$) is given by:

$$\vec{p} = q\vec{d} \tag{3.16}$$

Polarization (P) is referred to density of electric dipole moment. Polarization is important for the multiferroic materials. The measurements performed for the samples are discussed below.

The sintered cylindrical samples were electroded with silver as shown in fig. 3.8.

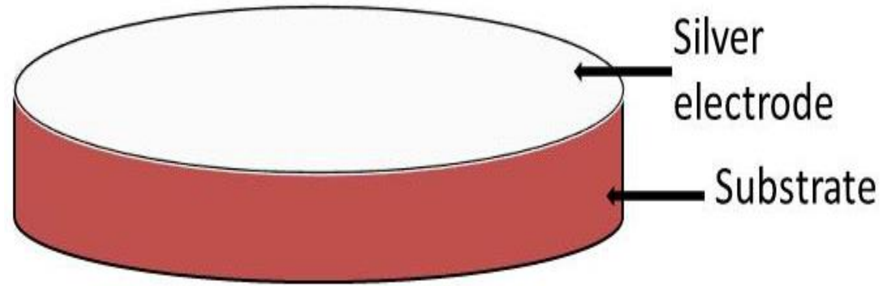

Fig. 3.9: Pellet used for Dielectric analysis.

3.2.3.1 Dielectric permittivity (ε_r):

Electric displacement field ($\vec{D}$): When a dielectric material is placed in an electric field (E), the bound charges get slightly displaced by a distance (d) which a local dipole moment is induced in the material.

$$\vec{D} \equiv \varepsilon_0 \mathrm{E} + \vec{P} = \varepsilon_0(1+\chi_e)\mathrm{E} = \varepsilon_r \varepsilon_0 \mathrm{E} \qquad (3.17)$$

Here, ε_r is relative dielectric permittivity also known as Dielectric constant. At zero frequency, it is named as static dielectric permittivity, χ_e electric susceptibility.

The capacitance C is defined as:

$$\mathrm{C} = \varepsilon_r \varepsilon_0 \frac{\mathrm{a}}{\vec{d}} \qquad (3.18)$$

Electric modulus: It is reciprocal of dielectric permittivity and defined as:

$$M(\omega) = \frac{1}{\varepsilon} = M' + \iota M'' = \frac{\varepsilon\prime(\omega)}{\varepsilon'(\omega)^2 + \varepsilon\prime\prime(\omega)^2} + \iota \frac{\varepsilon\prime\prime(\omega)}{\varepsilon'(\omega)^2 + \varepsilon\prime\prime(\omega)^2} \qquad (3.19)$$

For anisotropic materials, when analyzing the response of materials to ac conductivity is replaced with complex conductivity.

Complex conductivity is defined according to the equation as:

$$\sigma = \sigma' + \sigma_0 + \iota\sigma'' = \iota\omega\varepsilon_0\varepsilon \quad (3.20)$$

Where, σ_0 is dc conductivity, σ' is ac conductivity, ω is field frequency.

In this thesis work ac conductivity is calculated by following equation:

$$\sigma = \varepsilon''\varepsilon_0\omega \quad (3.21)$$

DC conductivity is highly temperature dependent and frequency independent. It is related with hopping transition and calculated with equation:

$$\sigma_{DC}T = \sigma_0 \, exp\left(\frac{-E}{k_B T}\right) \quad (3.22)$$

Dielectric Relaxation: It is response of non-interacting electrical dipoles to the applied external field. It is function of complex dielectric.

$$\varepsilon = \varepsilon'(\omega) - \iota\varepsilon''(\omega) \quad (3.23)$$

$$\varepsilon = \varepsilon_\infty + \frac{\varepsilon_0 - \varepsilon_\infty}{1 + \iota\omega\tau} \quad (3.24)$$

Here ε_0 and ε_∞ are the static and high frequency limit dielectric permittivity respectively. τ is the character relaxation time which is the function of temperature:

$$\tau = \tau_0 e^{E/kT} \quad (3.25)$$

3.2.3.2 Maxwell-Wagner relaxation

It accounts for the accumulation of charge at the two-material interface basis on the difference of charge carriers in relaxation times in these two materials, basic electrical

properties of materials are specified using two physical parameters, dielectric constant ε and conductivity σ as shown in Fig. 3.8. The ratio of these two parameters, $\tau = \frac{\varepsilon}{\sigma}$, gives relaxation time and stands for spreading time of excess free carriers in the materials.

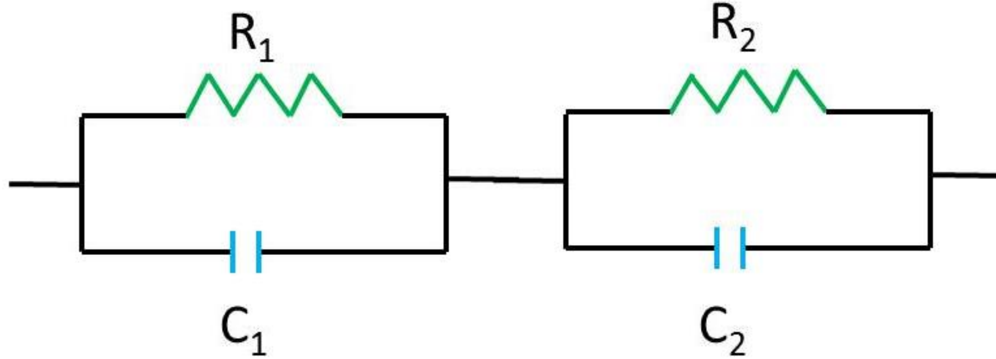

Fig. 3.10: Two layer electric circuit diagram for Maxwell relaxation.

$$\varepsilon = \varepsilon_\infty + \frac{\varepsilon_0 - \varepsilon_\infty}{1 + \iota\omega\tau} - \iota\frac{\sigma}{\omega} \tag{3.26}$$

Parameters related to circuit are as:

$$\varepsilon = \varepsilon_\infty + \frac{1}{C_0}\left(\frac{1}{\frac{1}{C_1}+\frac{1}{C_2}}\right) \tag{3.27}$$

$$\varepsilon_0 = \frac{R_1^2 C_1 + R_2^2 C_2}{C_0 (R_1 + R_2)^2} \tag{3.28}$$

$$\sigma = \frac{1}{C_0 (R_1 + R_2)} \tag{3.29}$$

$$\tau = \frac{R_1 R_2 (C_1 + C_2)}{R_1 + R_2} \tag{3.30}$$

$$C_0 = \frac{\varepsilon_0 a}{\vec{d}} \tag{3.31}$$

$$Z' = \frac{R_1}{1 + (\omega R_1 C_1)^2} + \frac{R_2}{1 + (\omega R_2 C_2)^2} \tag{3.32}$$

$$Z'' = R_1\left[\frac{\omega R_1 C_1}{1+(\omega R_1 C_1)^2}\right] + R_2\left[\frac{\omega R_2 C_2}{1+(\omega R_2 C_2)^2}\right] \quad (3.33)$$

$$M' = \frac{C_0}{C_1}\left[\frac{(\omega R_1 C_1)^2}{1+(\omega R_1 C_1)^2}\right] + \frac{C_0}{C_2}\left[\frac{(\omega R_2 C_2)^2}{1+(\omega R_2 C_2)^2}\right] \quad (3.34)$$

$$M'' = \frac{C_0}{C_1}\left[\frac{\omega R_1 C_1}{1+(\omega R_1 C_1)^2}\right] + \frac{C_0}{C_1}\left[\frac{\omega R_2 C_2}{1+(\omega R_2 C_2)^2}\right] \quad (3.35)$$

Dielectric room temperature measurement is done using impedance analyzer (Key Sight Technology, Model–E4990A, Malaysia. The high temperature measurement was performed with Solartron impedance analyzer (Model -1260A, United Kingdom).

3.2.5 Ferroelectric Measurement

It is a measurement system to prove the ferroelectricity by reversal of spontaneous polarization on application of electric field.

Poling: The purpose of poling is to make a material anisotropic by applying an external electric field which tends to domains aligned in the same direction of field and the removal of field leave a net remanent polarization.

In this thesis work the sintered pellets of thickness ~1mm were silver coated both sides and then polled at room temperature by placing the pellets in the silicon oil with a DC poling unit (Marine India), having voltage limit of 5kV.

P-E loop measurement setup, MARINE PE–0, was used to get ferroelectric hysteresis loop by using Sawyer-Tower (ST) electric circuit, in which variable capacitance (C_v) and variable resistance (R_v) of the circuit varied at fixed frequency 50Hz. The ST circuit is shown in Fig. 3.10.

So the polarization (P)

$$P = \frac{V_c}{a} - \varepsilon_0 E \quad (3.36)$$

Here, V_c is voltage of constant capacitor, a is the area of coated surface.

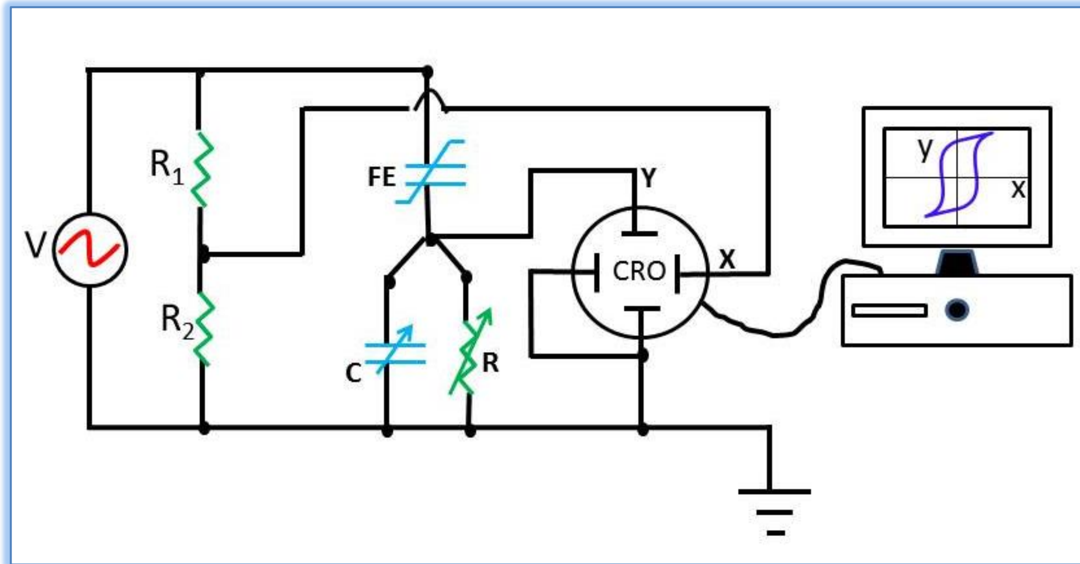

Fig. 3.11: Sawyer-Tower electric circuit diagram for ferroelectric hysteresis loop measurement.

3.2.6 Magnetic Studies

Magnetic measurement is performed with the superconducting quantum interference device (SQUID). It is highly sensitive fluxmeter, which measures the magnetic behavior of the samples when subjected to different temperatures, pressures, and change in the magnetic field. In SQUID, vacuum is created by liquid helium and the temperature inside the chamber is maintained with the liquid nitrogen. The sensitivity of the instrument is highly maintained by holding the magnetic field constant by a superconducting shield. The sample of specific size (2mm×2mm×4mm), fixed with a varnish in tufnol holder positioned at the end of a carbon rod between the two pick up coils, the sample moved slowly through the pickup coils and the quanta are counted.

Then the magnetic field is applied it moved through the coil in a series of 32 steps. To convert the signal into electromagnetic unit (emu), the sample is moved to a fixed distance 4cm and the generated signal is measured. A schematic diagram of SQUID is shown in Fig. 3.11.

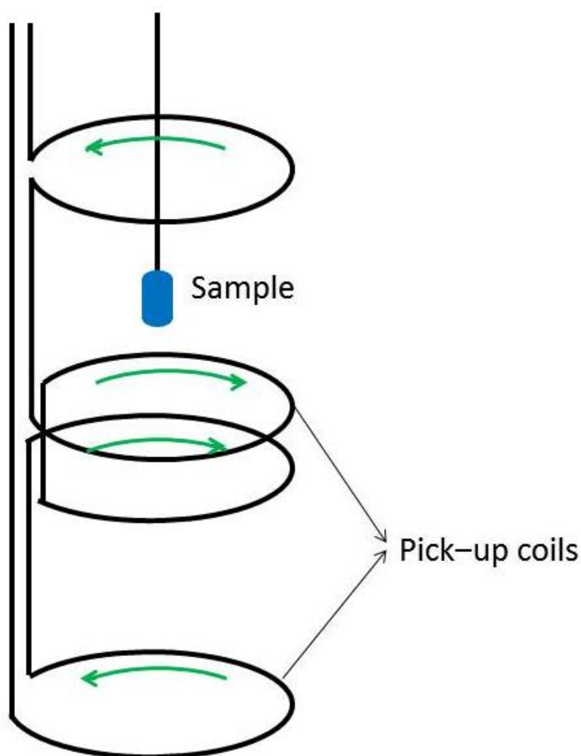

Fig. 3.12: Working principle of MPMS.

In this thesis work SQUID magnetometer of Quantum design, Model–MPMS 3, EM–QM, USA was used. It has range of field ±7T (tesla).

3.2.7 X-ray photoelectron spectroscopy

X-ray photoelectric absorption is based on photoelectric effect (ejection of electrons from a material when an electromagnetic radiation strikes to its surface) as shown in Fig. 3.12. In this technique x-ray beam irradiated on the sample surface and the ejected electrons provides

the information of present elements. XPS study also applied for line profiling of elemental composition [Greczynski *et al.* 2020].

XPS requires ultra-high vacuum ($p < 10^{-7}$ Pa) conditions. XPS can detects all elements except hydrogen and helium. The detection limit is in the parts per thousand range, but parts per million (ppm) are achievable with long collection times and concentration at top surface.

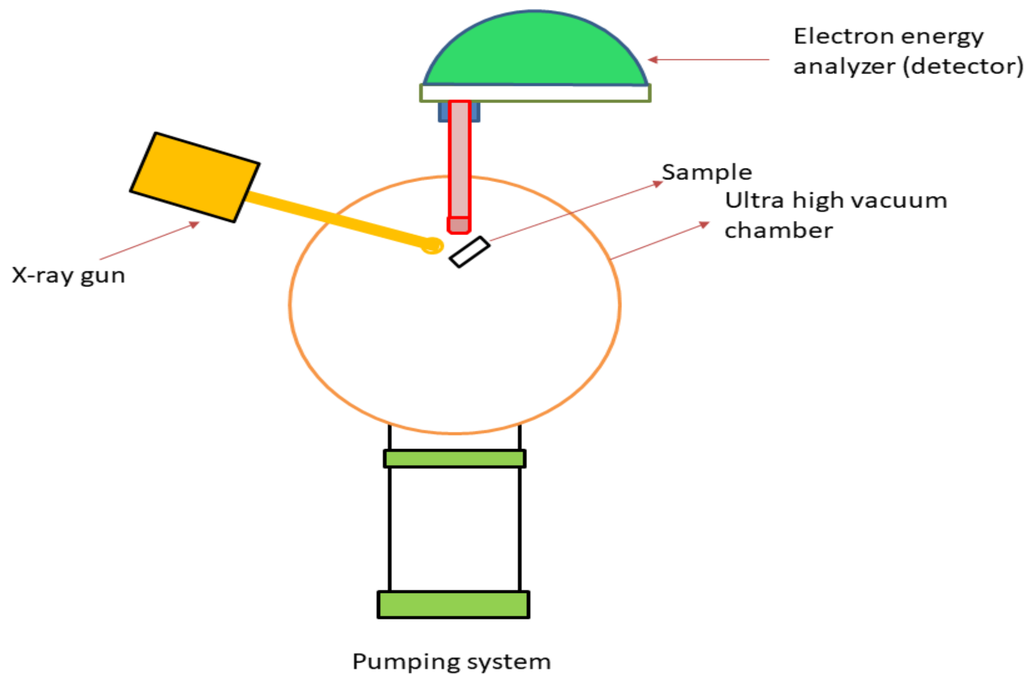

Fig. 3.13: Systematic diagram of XPS

XPS is routinely used to analyse inorganic compounds, semiconductors, metal alloys, polymers, glasses, ceramics, paints, papers, inks, woods, plant parts, bio-materials, viscous oils, glues, ion-modified materials, hydrated forms of materials (hydrogels) and many others.

In this thesis work XPS spectra that provide valence state and vacancy of the elements were recorded with X-ray photoelectron spectroscopy (K-alpha Thermo Fisher Scientific) in an inert atmosphere.

3.2.8 I-V characteristics (Leakage current)

The current-voltage characteristic is a destructive technique in which voltage is applied across the sample in order to determine the leakage phenomenon occurring inside the fabricated device, prior to the breakdown. To perform the testing, the voltage ranging from -10V to +10V applied across the two terminals of silver electroded samples. In this study for I-V characteristics measurement of the samples Keithley Source meter 2450 was used.